SUBSPACE-BASED DIRECTION-OF-ARRIVAL ESTIMATION FOR MORE SOURCES THAN SENSORS USING PLANAR ARRAYS

Michael Rübsamen *Alex B. Gershman*

Communication Systems Group
Darmstadt University of Technology
Merckstrasse 25, 64283 Darmstadt, Germany

ABSTRACT

We propose a novel subspace-based direction-of-arrival (DOA) estimation method and an associated planar array geometry optimization technique. The proposed DOA estimation approach allows to estimate the DOAs of more sources than sensors and to resolve manifold ambiguities in the case of uncorrelated signals. It is related to the covariance augmentation (CA) technique, but in contrast to the CA technique, it can be applied to non-uniform planar array geometries.

Index Terms— Direction-of-arrival estimation, covariance augmentation technique, planar arrays, manifold ambiguities

1. INTRODUCTION

Nonuniform linear arrays (NLAs) are widely used for DOA estimation, because such arrays can provide an increased aperture size as compared to uniform linear arrays (ULAs) with the same number of sensors. Therefore, NLAs can provide a substantially improved spatial resolution capability as compared to ULAs. However, if the aperture size of an NLA is larger than $(N-1)\lambda/2$, where λ is the signal wavelength and N denotes the number of sensors, then manifold ambiguities can occur [1]. These ambiguities lead to a breakdown of subspace-based DOA estimation techniques such as the multiple signal classification (MUSIC) algorithm [2, 3]. For specific classes of NLAs, e.g. for fully augmentable minimum redundancy arrays (MRAs), this performance breakdown can be avoided by means of the CA technique if the impinging source signals are uncorrelated [4, 5]. Furthermore, this technique allows to estimate the DOAs of more uncorrelated sources than sensors. The CA technique can be generalized to planar array geometries, but the sensors are required to lie on a uniform grid.

In this paper, we propose an alternative DOA estimation technique, which also allows to estimate the DOAs of more sources than sensors (the case called in [6] *"superior case DOA estimation"*) and to resolve manifold ambiguities if the signals are uncorrelated. However, our technique can be applied to non-uniform planar array geometries. We also propose an associated planar array geometry optimization technique, and demonstrate by an example that this technique leads to arrays with rather large aperture sizes and, correspondingly, good spatial resolution capability.

The proposed DOA estimation approach first computes an extended Toeplitz covariance matrix, which corresponds to so-called *virtual* Vandermonde steering vectors that contain in their elements the conventional Fourier basis functions. Subsequently, the source DOAs are estimated by applying a root-MUSIC-type algorithm to the Fourier domain covariance matrix [7]. The proposed technique is hereafter referred to as Fourier domain covariance augmentation (FDCA) technique.

This work was supported by the European Research Council (ERC) Advanced Investigator Grants Program under Grant 227477-ROSE.

2. BACKGROUND

Let us assume that L narrowband signals from far-field sources impinge on a planar array of N omnidirectional sensors. The $N \times 1$ array snapshot vector at time k can be modeled as [8]

$$\boldsymbol{x}(k) = \boldsymbol{A}(\boldsymbol{\theta})\boldsymbol{s}(k) + \boldsymbol{n}(k), \tag{1}$$

where the $L \times 1$ vector $\boldsymbol{\theta} = [\theta_1, \ldots, \theta_L]^T$ contains the unknown signal DOAs, $\boldsymbol{A}(\boldsymbol{\theta}) = [\boldsymbol{a}(\theta_1), \ldots, \boldsymbol{a}(\theta_L)]$ is the $N \times L$ steering matrix, $\boldsymbol{s}(k)$ is the $L \times 1$ signal waveform vector, $\boldsymbol{n}(k)$ is the $N \times 1$ noise vector, and $(\cdot)^T$ denotes the transpose. The nth component of the $N \times 1$ steering vector can be expressed as

$$a_n(\theta) = e^{j\frac{2\pi}{\lambda}(x_n \sin\theta + y_n \cos\theta)}, \tag{2}$$

where $\{x_n, y_n\}$ are the coordinates of the nth array sensor, θ is the steering angle, and $j = \sqrt{-1}$. In the following, the array manifold and the number of signals are assumed to be known.

The components of $\boldsymbol{s}(k)$ and $\boldsymbol{n}(k)$ are modeled as independent zero-mean circularly symmetric complex Gaussian random variables. The $N \times N$ array covariance matrix can be expressed as [8]

$$\boldsymbol{R}_{\boldsymbol{x}} \triangleq \mathrm{E}(\boldsymbol{x}(k)\boldsymbol{x}^H(k)) = \sum_{l=1}^{L} \boldsymbol{a}(\theta_l)\boldsymbol{a}^H(\theta_l)P_l + \sigma^2\boldsymbol{I}_N, \tag{3}$$

where P_l is the power of the lth signal, σ^2 is the noise power, $\boldsymbol{I}_N$ is the $N \times N$ identity matrix, and $\mathrm{E}(\cdot)$ and $(\cdot)^H$ stand for the statistical expectation and the Hermitian transpose, respectively. Note that the signals are assumed to be uncorrelated.

In practice, the array covariance matrix is unknown, but can be estimated from the received snapshot vectors as

$$\boldsymbol{C}_{\boldsymbol{x}} \triangleq \frac{1}{K}\sum_{k=1}^{K} \boldsymbol{x}(k)\boldsymbol{x}^H(k) = \boldsymbol{R}_{\boldsymbol{x}} + \boldsymbol{\Delta}, \tag{4}$$

where $\boldsymbol{\Delta}$ denotes the covariance estimation error.

If $L < N$, then the conventional MUSIC algorithm allows to estimate the signal DOAs by searching for the L smallest minima of the MUSIC null-spectrum function [2, 3]

$$f(\theta) \triangleq \boldsymbol{a}^H(\theta)\big(\boldsymbol{I}_N - \hat{\boldsymbol{E}}_S\hat{\boldsymbol{E}}_S^H\big)\boldsymbol{a}(\theta), \tag{5}$$

where the $N \times L$ matrix $\hat{\boldsymbol{E}}_S$ contains the L orthonormal principal eigenvectors of $\boldsymbol{C}_{\boldsymbol{x}}$. If the steering vectors $\boldsymbol{a}(\theta)$ have the Vandermonde structure, then the search over the MUSIC null-spectrum function can be replaced by a rooting technique, which provides an improved performance in scenarios with low signal-to-noise-ratios (SNRs) and/or closely spaced signals [7, 9].

3. FOURIER DOMAIN COVARIANCE AUGMENTATION TECHNIQUE

The steering vector components $a_n(\theta)$ are elements of the vector space $L_2^{(2\pi)}$ of 2π-periodic continuously differentiable functions with finite norm [10]

$$\|h(\theta)\|_2 \triangleq \left(\int_{-\pi}^{\pi} |h(\theta)|^2 \mathrm{d}\theta \right)^{1/2}. \tag{6}$$

The Fourier basis functions

$$g^m(\theta) \triangleq e^{jm\theta}, \quad m = -\infty, \ldots, \infty \tag{7}$$

form an orthogonal basis of $L_2^{(2\pi)}$. Let

$$\mathcal{S}_{\boldsymbol{a}} \triangleq \left\{ h(\theta) \,|\, h(\theta) = \boldsymbol{\alpha}^H \boldsymbol{a}(\theta),\ \boldsymbol{\alpha} \in \mathbb{C}^{N\times 1} \right\} \subset L_2^{(2\pi)} \tag{8}$$

denote the subspace that is spanned by the components of $\boldsymbol{a}(\theta)$. Clearly, this subspace depends on the sensor locations.

Let us briefly review a result for uniform circular arrays (UCAs) with $\lambda/2$-spacing between adjacent sensors. Let $\boldsymbol{a}_{\mathrm{UCA}}(\theta)$ denote the $N \times 1$ UCA steering vector. It has been shown in [11] that the Fourier basis functions $g^m(\theta)$ with $|m| < N/2$ lie approximately in the subspace that is spanned by the components of $\boldsymbol{a}_{\mathrm{UCA}}(\theta)$. Hence, we can write

$$g^m(\theta) \approx \boldsymbol{\alpha}_m^H \boldsymbol{a}_{\mathrm{UCA}}(\theta) \quad \forall\, |m| < N/2, \tag{9}$$

where $\boldsymbol{\alpha}_m$ is an $N \times 1$ weight vector. For $|m| \geq N/2$, this is no longer possible. As the dimension of the subspace that is spanned by the components of $\boldsymbol{a}_{\mathrm{UCA}}(\theta)$ is less than or equal to N, at most N Fourier basis functions can lie within this subspace.

It directly follows from (3) that for arbitrary array geometries

$$\mathrm{vec}(\boldsymbol{R}_{\boldsymbol{x}}) = \sum_{l=1}^{L} P_l \boldsymbol{b}(\theta_l) + \sigma^2 \mathrm{vec}(\boldsymbol{I}_N), \tag{10}$$

where $\mathrm{vec}(\cdot)$ is the vectorization operator that stacks the columns of a matrix on top of each other, and $\boldsymbol{b}(\theta) \triangleq \mathrm{vec}(\boldsymbol{a}(\theta)\boldsymbol{a}^H(\theta))$ is an $N^2 \times 1$ vector. The components of $\boldsymbol{b}(\theta)$ can be expressed as

$$b_{k+(l-1)N}(\theta) = e^{j\frac{2\pi}{\lambda}((x_k - x_l)\sin\theta + (y_k - y_l)\cos\theta)} \in L_2^{(2\pi)}. \tag{11}$$

Hence, these components depend on the displacements between the sensors. Let $\mathcal{S}_{\boldsymbol{b}}$ denote the subspace that is spanned by the components of $\boldsymbol{b}(\theta)$. As there are at most $D \triangleq N^2 - N + 1$ different sensor displacements, the dimension of $\mathcal{S}_{\boldsymbol{b}}$ is at most D. Since $D \gg N$, it can be expected that significantly more than N Fourier basis functions can be made to approximately lie within $\mathcal{S}_{\boldsymbol{b}}$ by an appropriate choice of the sensor locations. Then, $N^2 \times 1$ extended weight vectors $\boldsymbol{w}_m$ can be determined so that

$$g^m(\theta) = \boldsymbol{w}_m^H \boldsymbol{b}(\theta) + \delta_m(\theta) \quad \forall\, |m| < M, \tag{12}$$

where $M \gg N$, and $\delta_m(\theta)$ is a small approximation error. As the Fourier basis functions are orthogonal, an upper bound on M directly follows from $2M - 1 \leq D$. The choice of sensor locations and weight vectors $\boldsymbol{w}_m$ will be discussed in Section 4.

Let the $M \times M$ matrix $\tilde{\boldsymbol{R}}_{\boldsymbol{x}}$ be defined as

$$\tilde{\boldsymbol{R}}_{\boldsymbol{x}} \triangleq \sum_{l=1}^{L} P_l \tilde{\boldsymbol{a}}(\theta_l) \tilde{\boldsymbol{a}}^H(\theta_l), \tag{13}$$

where $\tilde{\boldsymbol{a}}(\theta) \triangleq [1, g(\theta), g^2(\theta), \ldots, g^{M-1}(\theta)]^T$ is an $M \times 1$ Vandermonde vector, which can be interpreted as a virtual steering vector. The superscript $\tilde{}$ is used to indicate Fourier domain variables. Since $\tilde{\boldsymbol{R}}_{\boldsymbol{x}}$ is Toeplitz and Hermitian, it is fully determined by the entries in its first column. It directly follows from (10) and (12) that the $(m+1)$th entry in the first column of $\tilde{\boldsymbol{R}}_{\boldsymbol{x}}$ can be expressed as

$$\begin{aligned} \left[\tilde{\boldsymbol{R}}_{\boldsymbol{x}}\right]_{m+1,1} &= \textstyle\sum_{l=1}^{L} P_l g^m(\theta_l) \\ &= \boldsymbol{w}_m^H \mathrm{vec}(\boldsymbol{R}_{\boldsymbol{x}} - \sigma^2 \boldsymbol{I}_N) + \sum_{l=1}^{L} P_l \delta_m(\theta_l). \end{aligned} \tag{14}$$

Assuming that the sensor noise power is known, $[\tilde{\boldsymbol{R}}_{\boldsymbol{x}}]_{m+1,1}$ can be estimated as

$$\left[\tilde{\boldsymbol{C}}_{\boldsymbol{x}}\right]_{m+1,1} \triangleq \boldsymbol{w}_m^H \mathrm{vec}(\boldsymbol{C}_{\boldsymbol{x}} - \sigma^2 \boldsymbol{I}_N), \tag{15}$$

where the approximation error is given by

$$\left[\tilde{\boldsymbol{C}}_{\boldsymbol{x}} - \tilde{\boldsymbol{R}}_{\boldsymbol{x}}\right]_{m+1,1} = \boldsymbol{w}_m^H \mathrm{vec}(\boldsymbol{\Delta}) - \sum_{l=1}^{L} P_l \delta_m(\theta_l), \tag{16}$$

and $\tilde{\boldsymbol{C}}_{\boldsymbol{x}}$ is an $M \times M$ Hermitian Toeplitz estimate of $\tilde{\boldsymbol{R}}_{\boldsymbol{x}}$. The essence of the proposed FDCA technique is to estimate the source DOAs by applying the root-MUSIC algorithm to $\tilde{\boldsymbol{C}}_{\boldsymbol{x}}$.

Note that $L \leq M$ pairwise different vectors $\tilde{\boldsymbol{a}}(\theta)$ are always linearly independent due to the Vandermonde structure of these vectors. As $g(\theta)$ is one-to-one on the interval $[-\pi, \pi)$, virtual manifold ambiguities cannot occur if $L < M$. Consequently, the root-MUSIC algorithm allows to exactly recover the source DOAs from $\tilde{\boldsymbol{R}}_{\boldsymbol{x}}$ if $L < M$. Hence, if $\tilde{\boldsymbol{C}}_{\boldsymbol{x}}$ is a sufficiently accurate estimate of $\tilde{\boldsymbol{R}}_{\boldsymbol{x}}$, then the FDCA technique can estimate up to $M - 1$ source DOAs. In particular, the FDCA technique allows to estimate more source DOAs than sensors if $M > N + 1$.

A manifold ambiguity occurs if $\mathcal{R}(\boldsymbol{A}(\boldsymbol{\theta})) = \mathcal{R}(\boldsymbol{A}(\bar{\boldsymbol{\theta}}))$, where $\bar{\boldsymbol{\theta}} = [\bar{\theta}_1, \ldots, \bar{\theta}_L]^T$ is another vector of $L < N$ DOAs with at least one DOA that is not contained in $\boldsymbol{\theta}$, and $\mathcal{R}(\cdot)$ is the column space operator. In this case, the MUSIC null-spectrum function of $\boldsymbol{R}_{\boldsymbol{x}}$ has nulls at all angles θ_l and $\bar{\theta}_l$, $l = 1, \ldots, L$. The spurious nulls lead to outliers among the DOA estimates of the MUSIC algorithm applied to $\boldsymbol{C}_{\boldsymbol{x}}$. However, such an ambiguity does not occur for the virtual steering vectors if $M \geq N$, because $L + 1 \leq M$ different Vandermonde vectors $\tilde{\boldsymbol{a}}(\theta)$ are always linearly independent. Consequently, $\mathcal{R}(\tilde{\boldsymbol{A}}(\boldsymbol{\theta})) \neq \mathcal{R}(\tilde{\boldsymbol{A}}(\bar{\boldsymbol{\theta}}))$, where $\tilde{\boldsymbol{A}}(\boldsymbol{\theta}) \triangleq [\tilde{\boldsymbol{a}}(\theta_1), \ldots, \tilde{\boldsymbol{a}}(\theta_L)]$ is the $M \times L$ virtual steering matrix. The FDCA technique therefore allows to resolve manifold ambiguities, similar to the CA technique [5].

The DOA estimation mean-square-error (MSE) performance of the CA technique is often significantly worse than the stochastic Cramér-Rao lower bound (CRLB) due to estimation errors in the augmented covariance matrix [6]. As the CA and FDCA techniques construct extended Toeplitz covariance matrices in a similar way, it can be expected that also the FDCA technique does not achieve the stochastic CRLB. However, the DOA estimates of both the CA and FDCA techniques can be refined efficiently by a local maximization of the likelihood function as suggested in [6] in application to the CA approach.

4. ARRAY GEOMETRY OPTIMIZATION

The performance of the FDCA technique depends on the accuracy and the dimensionality of $\tilde{\boldsymbol{C}}_{\boldsymbol{x}}$. We first discuss the optimization of the array geometry and weight vectors $\boldsymbol{w}_m$ for a fixed value of M, and subsequently discuss the choice of M.

One approach to achieve a small approximation error in (16) is by minimizing the norm of $\boldsymbol{w}_m$ subject to the constraint that $\|\delta_m(\theta)\|_2 \leq \epsilon_m \|g^m(\theta)\|_2$, where ϵ_m is a user-defined parameter which controls the approximation accuracy. To formulate the latter constraint in a finite convex form, let us sample $g^m(\theta)$ and $\boldsymbol{b}(\theta)$ at $\breve{\theta}_t = 2\pi(t-1)/T$ for $t = 1, \ldots, T$. Using (12) and the notations

$$\boldsymbol{g}_m \triangleq [g^m(\breve{\theta}_1), \ldots, g^m(\breve{\theta}_T)] \text{ and } \boldsymbol{B} \triangleq [\boldsymbol{b}(\breve{\theta}_1), \ldots, \boldsymbol{b}(\breve{\theta}_T)],$$

we obtain the constraint

$$\|\boldsymbol{g}_m - \boldsymbol{w}_m^H \boldsymbol{B}\|_2 \leq \epsilon_m \sqrt{T}, \tag{17}$$

where $\|\cdot\|_2$ in (17) denotes the Euclidean vector norm. The parameter T has to be chosen sufficiently large such that the Nyquist sampling criterion is satisfied for $g^m(\theta)$ and all components of $\boldsymbol{b}(\theta)$. Note that (17) can be satisfied if and only if

$$\|\boldsymbol{g}_m(\boldsymbol{I}_T - \boldsymbol{P}_{\boldsymbol{B}^H})\|_2 \leq \epsilon_m \sqrt{T}, \tag{18}$$

where $\boldsymbol{P}_{\boldsymbol{B}^H}$ is the orthogonal projection matrix onto $\mathcal{R}(\boldsymbol{B}^H)$.

The array geometry and weight vectors $\boldsymbol{w}_m$ can be optimized jointly by solving

$$\begin{array}{ll} \min\limits_{\boldsymbol{d}_x, \boldsymbol{d}_y, \boldsymbol{w}_m} & \sum_{m=0}^{M-1} \|\boldsymbol{w}_m\|_2 \\ \text{s.t.} & \|\boldsymbol{g}_m - \boldsymbol{w}_m^H \boldsymbol{B}(\boldsymbol{d}_x, \boldsymbol{d}_y)\|_2 \leq \epsilon_m \sqrt{T} \\ & \forall\ m = 0, \ldots, M-1, \end{array} \tag{19}$$

where we emphasize for clarity the dependency of $\boldsymbol{B}$ on $\boldsymbol{d}_x \triangleq [x_1, \ldots, x_N]^T$ and $\boldsymbol{d}_y \triangleq [y_1, \ldots, y_N]^T$. For fixed values of $\boldsymbol{d}_x$ and $\boldsymbol{d}_y$, the optimization of the weight vectors $\boldsymbol{w}_m$ is a convex problem, which can be solved efficiently by M one-dimensional searches over Lagrange parameters. The minimization with respect to $\boldsymbol{d}_x$ and $\boldsymbol{d}_y$ is a non-convex problem. In our simulations, we employ an evolutionary algorithm to obtain (locally) optimum values for $\boldsymbol{d}_x$ and $\boldsymbol{d}_y$. Note that (19) is typically optimized off-line, so the high computational complexity involved with the genetic search is not a severe practical limitation. Furthermore, note that (19) can be modified straightforwardly to take into account application-specific constraints on the sensor locations.

As explained in Sec. 3, the value of M should be as large as possible, provided that a close approximation of $\tilde{\boldsymbol{R}}_{\boldsymbol{x}}$ can be obtained. However, (19) may be infeasible or feasible only for large norms of $\boldsymbol{w}_m$ if M is chosen too large. Therefore, we search for solutions of (19) for different values of M, and choose the result for the maximum M such that all norms of $\boldsymbol{w}_m$ are below some user-defined threshold ξ. Note that the conventional CA technique uses similar weight vectors with norm $1/\sqrt{J}$, where J is the degree of redundancy, which is typically equal to one for an MRA. Hence, ξ may be chosen heuristically as $1 \ldots 5$.

The Fourier series expansion allows to write

$$b_{k+(l-1)N}(\theta) = \sum_{m=-\infty}^{\infty} \beta_m^{(k,l)} g^m(\theta), \tag{20}$$

where the Fourier series coefficients are given by [10]

$$\beta_m^{(k,l)} \triangleq \frac{1}{2\pi} \int_{-\pi}^{\pi} b_{k+(l-1)N}(\theta) g^{-m}(\theta) \mathrm{d}\theta. \tag{21}$$

If the distance between the kth and the lth sensor locations is small, then $|\beta_m^{(k,l)}|$ decreases rapidly with increasing $|m|$. Hence, if M is large and if all distances between the sensors are small, then it is impossible to approximate $g^{M-1}(\theta)$ with a small norm of $\boldsymbol{w}_{M-1}$. Vice versa, a large value of M implicitly enforces a large sensor array aperture.

From (14), we obtain

$$\left[\tilde{\boldsymbol{R}}_{\boldsymbol{x}}\right]_{m+1,1} = \int_{-\pi}^{\pi} \Phi(\theta) g^m(\theta) \mathrm{d}\theta, \tag{22}$$

where

$$\Phi(\theta) = \sum_{l=1}^{L} P_l \delta(\theta - \theta_l) \tag{23}$$

is the angular power density, and $\delta(\theta)$ is the Dirac delta. Consequently, the components of $\tilde{\boldsymbol{R}}_{\boldsymbol{x}}/(2\pi)$ are Fourier series coefficients of $\Phi(\theta)$. The proposed array geometry optimization approach therefore attempts to maximize the number of Fourier series coefficients of $\Phi(\theta)$ that can be accurately estimated from $\boldsymbol{C}_{\boldsymbol{x}}$.

5. SIMULATION RESULTS

In this section, we evaluate the performance of the FDCA technique. We assume an array of $N = 9$ sensors. The array geometry and weight vectors $\boldsymbol{w}_m$ are determined as explained in Sec. 4 using $\epsilon_m = 10^{-2}$ for all m and $\xi = 3$.

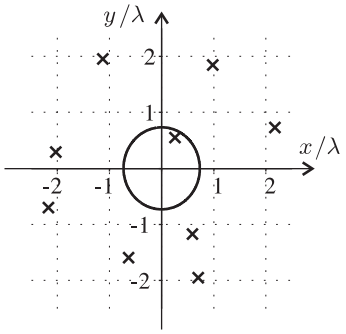

x_n/λ	y_n/λ
-2.170	-0.702
-2.029	0.289
-1.128	1.950
-0.631	-1.595
0.256	0.550
0.592	-1.172
0.702	-1.950
0.982	1.841
2.170	0.729

Fig. 1. Array geometry (the sensor locations are depicted by the crosses). The circle shows as a reference the size of a UCA with the same number of sensors and $\lambda/2$ spacing between adjacent sensors.

Figure 1 depicts the sensor locations for $M = 24$. For comparison, we also draw the circle on which the sensors of a UCA with $\lambda/2$ spacing between adjacent sensors would be located. The comparison shows that the proposed array geometry has a rather large aperture size, and therefore provides improved spatial resolution capability as compared to the UCA with $\lambda/2$ spacing between adjacent sensors. The following simulation results are averaged over the sources.

In our first example, we consider the case of more signals than sensors. In this case, it is not possible to estimate the signal DOAs by applying the MUSIC algorithm to $\boldsymbol{C}_{\boldsymbol{x}}$. We assume that $L = 12$ equal-powered signals with SNR $= 0$ dB impinge on the sensor array from the DOAs $\theta_l = (l-1)15^\circ(\pi/180^\circ)$. Figure 2 shows that the FDCA technique reliably estimates all signal DOAs. As expected, the FDCA technique does not achieve the stochastic CRLB. The root-mean-square-error (RMSE) of the FDCA estimates is close to the standard deviation, so the approximation errors in (12) do not lead to significantly biased DOA estimates. Figure 2 also demonstrates that the RMSE performance of the refined FDCA estimates,

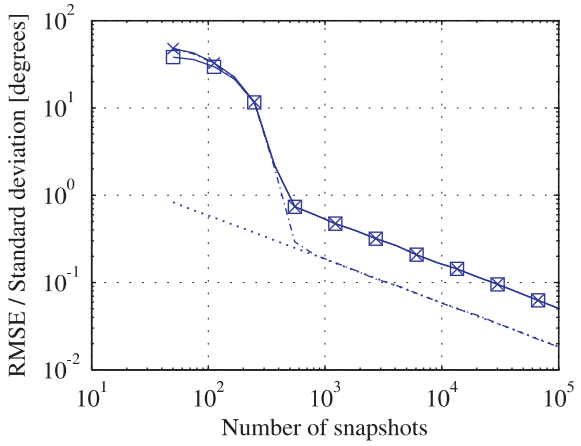

Fig. 2. DOA estimation performance for more sources than sensors. Solid line with crosses: RMSE of the FDCA estimates. Solid line with squares: Standard deviation of the FDCA estimates. Dash-dotted line: RMSE of the refined FDCA estimates, based on a local maximization of the likelihood function. Dotted line: Stochastic CRLB.

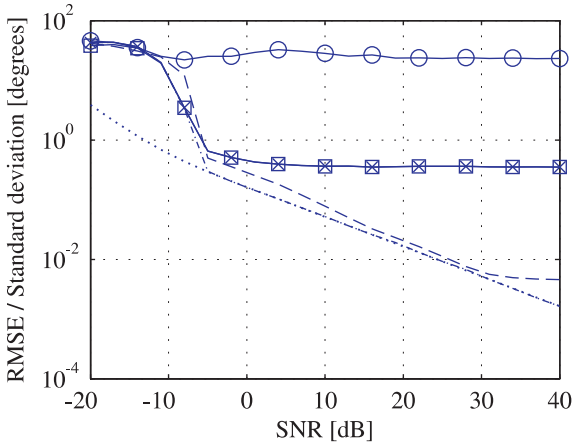

Fig. 3. DOA estimation performance in the case of manifold ambiguities. Solid line with crosses: RMSE of the FDCA estimates. Solid line with squares: Standard deviation of the FDCA estimates. Dash-dotted line: RMSE of the refined FDCA estimates, based on a local maximization of the likelihood function. Dashed line: RMSE of the Capon estimates. Solid line with circles: RMSE of the MUSIC estimates. Dotted line: Stochastic CRLB.

obtained by a local maximization of the likelihood function, is close to the stochastic CRLB.

In our second example, we consider a scenario with a manifold ambiguity. We assume $L = 6$ equal-powered sources with $\boldsymbol{\theta} = [-3.044, -1.584, -1.007, -0.296, 0.913, 1.324]^T$. A manifold ambiguity occurs, because $\boldsymbol{a}(1.586)$ lies approximately within $\mathcal{R}(\boldsymbol{A}(\boldsymbol{\theta}))$. Consequently, the MUSIC null-spectrum function of $\boldsymbol{R_x}$ has a spurious null at $\theta = 1.586$, which leads to outliers among the DOA estimates of the MUSIC algorithm. We compare the performance of the FDCA technique with the performance of the Capon DOA estimation technique [8]. The array covariance matrix is estimated using $K = 250$ independent snapshot vectors. Figure 3 demonstrates that the FDCA technique reliably resolves the manifold ambiguity, and that the local refinement of the FDCA estimates allows to efficiently obtain a DOA estimation performance that is close to the stochastic CRLB. However, Fig. 3 also shows that the Capon estimator outperforms the FDCA technique for most of the SNR values, which is typically the case in scenarios with less sources than sensors. The main benefit of the FDCA technique is therefore that it allows to estimate the DOAs of more sources than sensors.

6. CONCLUSION

The proposed subspace-based DOA estimation technique generalizes the conventional covariance augmentation technique to non-uniform planar array geometries. A new approach to the optimization of planar array geometries has been proposed based on our DOA estimation method. Simulation results show that the proposed technique allows to estimate the DOAs of more uncorrelated sources than sensors, using only second-order statistics of the received data.

7. REFERENCES

[1] A. Manikas and C. Proukakis, "Modeling and estimation of ambiguities in linear arrays," *IEEE Trans. Signal Processing*, vol. 46, pp. 2166-2179, Aug. 1998.

[2] R. O. Schmidt, "Multiple emitter location and signal parameter estimation," in *Proc. RADC Spectral Estimation Workshop*, Rome, NY, USA, Oct. 1979, pp. 243-258.

[3] G. Bienvenu and L. Kopp, "Adaptivity to background noise spatial coherence for high resolution passive methods," in *Proc. ICASSP'80*, Denver, CO, USA, Apr. 1980, pp. 307-310.

[4] S. U. Pillai, Y. Bar-Ness, and F. Haber, "A new approach to array geometry for improved spatial spectrum estimation," in *Proc. IEEE*, vol. 73, pp. 1522-1524, Oct. 1985.

[5] Y. I. Abramovich, N. K. Spencer, and A. Y. Gorokhov, "Resolving manifold ambiguities in direction-of-arrival estimation for nonuniform linear antenna arrays," *IEEE Trans. Signal Processing*, vol. 47, pp. 2629-2643, Oct. 1999.

[6] Y. I. Abramovich, D. A. Gray, A. Y. Gorokhov, and N. K. Spencer, "Positive-definite Toeplitz completion in DOA estimation for nonuniform linear antenna arrays — Part I: Fully augmentable arrays," *IEEE Trans. Signal Processing*, vol. 46, pp. 2458-2471, Sept. 1998.

[7] A. Barabell, "Improving the resolution performance of eigenstructure-based direction-finding algorithms," *Proc. ICASSP'83*, Boston, MA, USA, Apr. 1983, pp. 336-339.

[8] H. L. Van Trees, *Optimum Array Processing*. Wiley, 2002.

[9] B. D. Rao and K. V. S. Hari, "Performance analysis of root-MUSIC," *IEEE Trans. Acoust., Speech, Signal Processing*, vol. 37, pp. 1939-1949, Dec. 1989.

[10] W. Rudin, *Principles of Mathematical Analysis*. McGraw-Hill, 1976.

[11] C. P. Mathews and M. D. Zoltowski, "Eigenstructure techniques for 2-D angle estimation with uniform circular arrays," *IEEE Trans. Signal Processing*, vol. 42, pp. 2395-2407, Sept. 1994.